HHS Public Access

Author manuscript

*Nat Neurosci*. Author manuscript; available in PMC 2016 April 25.

Published in final edited form as:

*Nat Neurosci*. 2014 November ; 17(11): 1543–1551. doi:10.1038/nn.3823.

# Single rodent mesohabenular axons release glutamate and GABA

**David H. Root**[1,*], **Carlos Mejias-Aponte**[1,*], **Shiliang Zhang**[1,*], **Huiling Wang**[1], **Alexander F. Hoffman**[2], **Carl R. Lupica**[2], and **Marisela Morales**[1,+]

[1]Neuronal Networks Section, Integrative Neuroscience Research Branch, National Institute on Drug Abuse, 251 Bayview Blvd Suite 200, Baltimore, MD 21224

[2]Electrophysiology Research Section, Cellular Neurobiology Research Branch, National Institute on Drug Abuse, 333 Cassell Blvd, Baltimore, MD 21224

## Abstract

The lateral habenula (LHb) is involved in reward, aversion, addiction, and depression, through descending interactions with several brain structures, including the ventral tegmental area (VTA). VTA provides reciprocal inputs to LHb, but their actions are unclear. Here we show that the majority of rat and mouse VTA neurons innervating LHb co-express markers for both glutamate-signaling (vesicular glutamate transporter 2, VGluT2) and GABA-signaling (glutamate decarboxylase, GAD; and vesicular GABA transporter, VGaT). A single axon from these mesohabenular neurons co-expresses VGluT2-protein and VGaT-protein, and surprisingly establishes symmetric and asymmetric synapses on LHb neurons. In LHb slices, light activation of mesohabenular fibers expressing channelrhodopsin-2 (ChR2) driven by VGluT2 or VGaT promoters elicits release of both glutamate and GABA onto single LHb neurons. In vivo light-activation of mesohabenular terminals inhibits or excites LHb neurons. Our findings reveal an unanticipated type of VTA neuron that co-transmits glutamate and GABA, and provides the majority of mesohabenular inputs.

### Keywords

dopamine; reward; aversion; addiction; VGluT2; GAD; cotransmission; corelease



[+]Corresponding Author: Marisela Morales, Ph.D., Neuronal Networks Section, Integrative Neuroscience Research Branch, National Institute on Drug Abuse, 251 Bayview Blvd, Suite 200, Baltimore MD 21224, mmorales@intra.nida.nih.gov, 443-740-2717.
[*]These authors contributed equally to this work.

Author Contributions: All authors participated in the conception and design of experiments. HW and DHR performed retrograde tract tracing and *in situ* hybridization experiments. Cell counting was completed by HW, CAMA, and DHR. SZ performed and analysed confocal and electron microscopy experiments. AFH performed and AFH and CRL analysed whole-cell electrophysiological recording experiments. CAMA and DHR performed and analysed *in vivo* electrophysiological recording experiments. All authors contributed in writing the manuscript.

The authors declare that they do not have any conflicts of interest (financial or otherwise) related to the data presented in this manuscript.

Converging evidence demonstrates that descending LHb efferent pathways regulate VTA activity and play a prominent role in learning, motivation, reward, and aversion[1–11]. In contrast, the role of ascending VTA projections to the LHb are not well understood, although anatomical studies delineated this pathway over 30 years ago[12]. The detection of tyrosine hydroxylase [TH$^+$] fibers in the rat LHb originating from the VTA[13–14] has led to the assumption that dopamine (DA) from the VTA is released in the LHb, and the suggestion that DA plays a prominent role within this structure. However, anatomical studies in the rat show that the majority of VTA neurons targeting the LHb (mesohabenular neurons) lack TH[12,14–15], indicating that the mesohabenular inputs are mostly non-DAergic. In addition, recent mouse studies show that optogenetic stimulation of LHb fibers arising from VTA TH neurons results in the release of GABA without detectable release of DA[11]. Findings from other mouse studies suggest that some non-TH mesohabenular neurons may be glutamatergic, as VTA neurons expressing VGluT2 innervate the LHb[16–17]. These findings underscore the complexity of the VTA projections to the LHb whose molecular and synaptic composition are unclear. Here, we used a combination of tract tracing, molecular, microscopy, electrophysiological, pharmacological, and optogenetic techniques to identify: 1) the types of VTA neurons projecting to LHb; 2) the axon terminals and synaptic architectures that these neurons establish onto LHb neurons; 3) the neurotransmitter-release capacities of mesohabenular axon terminals; and 4) the firing patterns evoked in LHb neurons following activation of mesohabenular axon terminals. We found that 1) the majority of VTA neurons projecting to LHb belong to a previously unrecognized VTA neuronal phenotype that co-expresses transcripts encoding VGluT2 and GAD 65/67; 2) mesohabenular axon terminals belong to a previously unrecognized type of synaptic architecture in which a single axon terminal co-expresses VGluT2 and VGaT, establishes both asymmetric and symmetric synapses, expresses AMPA receptors postsynaptic to asymmetric synapses, and expresses $GABA_A$ receptors postsynaptic to symmetric synapses; 3) mesohabenular terminals monosynaptically co-transmit glutamate and GABA onto LHb neurons, a type of neurotransmission that had not been previously demonstrated in the adult mammalian brain; and 4) evoke inhibitory and excitatory changes in firing rate of LHb neurons *in vivo*.

## Results

### Most mesohabenular neurons are VGluT2$^+$

To determine the molecular composition of rat VTA projections to the LHb, we used a combination of neuroanatomical approaches. It has been established that TH$^+$ and TH$^-$ VTA neurons that innervate the LHb (mesohabenular neurons) are within the anteromedial VTA[12, 14–15,17]. Since this region contains many neurons that express VGluT2 mRNA[18] [VGluT2$^+$], we initially determined the degree of expression of TH-protein or VGluT2-mRNA within the mesohabenular neurons. Rat mesohabenular neurons were labeled *in vivo* by injection of the retrograde tracer FluoroGold (FG) into the LHb (Supplementary Fig. 1a, b). These FG neurons were phenotyped by a combination of immunolabeling (to detect TH) and radioactive *in situ* hybridization (to detect VGluT2 mRNA). Based on cellular expression of TH or VGluT2 within the FG-labeled neurons, we found 4 classes of mesohabenular neurons: VGluT2$^+$ TH$^-$ [67.6 ± 0.4%; 418/619]; VGluT2$^+$ TH$^+$ (24.9

± 0.3%; 154/619]; VGluT2$^{-}$ TH$^{+}$ [1.9 ± 0.5%; 12/619); and VGluT2$^{-}$ TH$^{-}$ [5.6 ± 0.5%; 35/619] (Supplementary Fig. 1c–j). These findings indicate that the major ascending projection from VTA to LHb consists of VGluT2$^{+}$ neurons (≈ 90%), with a minor pathway arising from a smaller population (≈ 25%) of TH$^{+}$ neurons. Although most of these VGluT2$^{+}$ mesohabenular neurons are TH$^{-}$, nearly all TH$^{+}$ neurons (≈ 90%) co-express VGluT2 mRNA. Together, these data suggest that the vast majority of mesohabenular neurons have the capacity to accumulate glutamate into synaptic vesicles via VGluT2.

## Most VGluT2$^{+}$ mesohabenular neurons are GAD$^{+}$

To determine whether the smaller population of VGluT2$^{-}$ mesohabenular neurons expressed GABAergic markers, we examined GAD65/67 mRNA expression in FG-labeled rat mesohabenular neurons using radioactive *in situ* hybridization. Surprisingly, we found that most mesohabenular neurons were GAD$^{+}$ [81.5% ± 0.4%; 513/630; Supplementary Fig. 2] with a frequency similar to that found for mesohabenular VGluT2$^{+}$ neurons, suggesting a significant overlap between these neuronal populations. To test this, and to determine the extent to which TH is expressed in this population of neurons, we applied a combination of dual fluorescent immunocytochemistry and dual *in situ* hybridization (radioactive and non-radioactive) techniques. We found that most of the mesohabenular neurons were dual VGluT2$^{+}$ GAD$^{+}$ [79.7% ± 2.1%; 382/477; Fig. 1], and ~70% were TH$^{-}$ [VGluT2$^{+}$ GAD$^{+}$ TH$^{-}$; 271/382]. In addition to these two major subpopulations of mesohabenular neurons, six other small subpopulations were found (Table 1 and Supplementary Fig. 3). The different phenotypes of mesohabenular neurons were intermingled within the anteromedial VTA (Supplementary Fig. 4). Thus the phenotypic characterization of mesohabenular neurons indicates that the major projection from VTA to LHb is from a novel population of VGluT2$^{+}$ GAD$^{+}$ co-expressing neurons that are able to accumulate vesicular glutamate and synthesize GABA.

## Most LHb axon terminals are VGluT2$^{+}$ VGaT$^{+}$

In order to determine if LHb neurons receive dual glutamatergic and GABAergic projections, rat LHb samples were processed for detection of VGluT2 and VGaT by immunoelectron microscopy. We identified three types of axon terminals with different frequencies (Supplementary Fig. 5): VGluT2$^{+}$ VGaT$^{-}$ axon terminals (33.5 ± 1.3%; 468/1410), VGluT2$^{-}$ VGaT$^{+}$ axon terminals (13.4 ± 1.5%; 194/1410) and VGluT2$^{+}$ VGaT$^{+}$ axon terminals (53.1 ± 0.9%; 748/1410). At the synapse level (Supplementary Fig. 5), single axon terminals form asymmetric synapses (putative excitatory[19]), symmetric synapses (putative inhibitory[19]) and puncta adhaerentia (adhesion sites between axon terminals[19–20]). Thus the LHb is the first recognized structure in which the majority of innervations are from dual glutamatergic-GABAergic neurons that form both symmetric and asymmetric synapses.

## Most mesohabenular axon terminals are VGluT2$^{+}$ VGaT$^{+}$

After establishing that the LHb has a large population of VGluT2$^{+}$ VGaT$^{+}$ axon terminals, we next used a transgenic mouse line to determine whether the VGluT2$^{+}$ GABA$^{+}$ mesohabenular neurons are a source of some of the VGluT2$^{+}$ VGaT$^{+}$ terminals present in the LHb. To selectively tag mesohabenular axon terminals derived from VTA VGluT2 neurons, a Cre-inducible adeno-associated vector (AAV) encoding channelrhodopsin2

(ChR2)-mCherry (AAV-DIO-ChR2-mCherry) was delivered into the VTA of VGluT2::Cre mice (VGluT2-ChR2-mCherry mice; Fig. 2a). By three-dimensional reconstruction of confocal images from triple fluorescent immunolabeled LHb, we found that the majority of mCherry-labeled mesohabenular axon terminals co-expressed VGluT2 and VGaT (69.07% ± 1.13%; 1415/2043; Figs. 2b–l). A smaller population of mesohabenular axon terminals contained VGluT2 without VGaT (28.18% ± 1.09%; 572/2043) or, VGaT without VGluT2 (2.8 ± 0.1%; 56/2043) (Fig. 2b–l). These findings indicate that the majority of axon terminals from mesohabenular VGluT2$^+$ GABA$^+$ neurons are endowed with the capability for vesicular accumulation of both glutamate and GABA within the same terminals. By immunoelectron microscopy we confirmed expression of VGluT2 in mCherry-labeled mesohabenular axon terminals (Fig. 2m). These mCherry-labeled VGluT2$^+$ terminals established asymmetric synapses with dendritic spines or dendrites, and synapsed with more than one postsynaptic structure (Fig. 2m; Supplementary Fig. 6). We also detected the expression of VGaT in mCherry-labeled mesohabenular axon terminals. As in the rat, some mouse mesohabenular terminals (Fig. 2n) exhibited puncta adhaerentia. Ultrathin serial section analysis of these terminals revealed that single mCherry-labeled VGaT$^+$ axon terminals established both asymmetric synapses and symmetric synapses on LHb neurons (Fig. 2n–p; Supplementary Fig. 7). These ultrastructural findings provide further evidence that VGluT2$^+$ GABA$^+$ mesohabenular neurons have the capacity to accumulate vesicular glutamate and GABA within the same axon terminals, and that these terminals can simultaneously establish asymmetric and symmetric synapses. VGluT2 and VGaT are likely sorted to individual vesicles[21], as emerging evidence indicates that these types of transporters have specific sorting signals determined by selective motifs within their molecular structures[22].

## Glutamate and GABA receptors are postsynaptic to mesohabenular terminals

We next applied confocal fluorescent and electron microscopy to determine if in the LHb glutamate and GABA receptors are postsynaptic to single mesohabenular axon terminals. By three-dimensional reconstruction of confocal images of triple fluorescent immunolabeled LHb, we found that mCherry-labeled mesohabenular axon terminals were present within the vicinity of both $GABA_A$ receptors and glutamate 1 AMPA receptors (GluR1) (Fig. 3a,b). By electron microscopy, we found that single mCherry-labeled mesohabenular axon terminals had GluR1 postsynaptic to their asymmetric synapses and $GABA_A$ receptors postsynaptic to their symmetric synapses (Fig. 3c,d). This arrangement of a single mesohabenular axon terminal establishing asymmetric synapses containing postsynaptic GluR1 and establishing symmetric synapses containing postsynaptic $GABA_A$ receptors was also observed in the rat LHb (Fig. 3e,f). From our anatomical findings, we concluded that in the mouse and in the rat, VTA projections to LHb are capable of accumulating vesicular glutamate and vesicular GABA within a single axon terminal that establishes asymmetric synapses with postsynaptic glutamate receptors and symmetric synapses with postsynaptic GABA receptors.

## Mesohabenular co-transmission of glutamate and GABA

The above detailed synaptic organization of mesohabenular axon terminals led us to hypothesize that mesohabenular terminals co-transmit glutamate and GABA onto LHb neurons. To test this hypothesis, we performed intracellular recordings from individual LHb

neurons in brain slices obtained from mice expressing ChR2-eYFP under the control of the VGluT2 promoter (VGluT2-ChR2 mice; Fig. 4a, b). Light stimulation (5 ms) of ChR2-eYFP mesohabenular fibers evoked synaptic currents that displayed both a fast inward current and a slower outward current in 8 of 9 recorded LHb neurons (6 VGluT2-ChR2 mice; Fig. 4c, d). LHb neurons were voltage-clamped at −70 mV (near the null potential for $Cl^-$) to isolate the inward synaptic current, and at −50 mV to isolate the outward current. The light-evoked inward current was selectively blocked by the AMPA-receptor antagonist NBQX (5 μM) without affecting the light-evoked outward current (Fig. 4d, summary in Fig. 5e). These findings indicate that the inward synaptic currents are mediated by glutamate transmission. In contrast, the $GABA_A$-receptor antagonist picrotoxin (50 μM) blocked the light-evoked outward currents (Fig 4c, summary in Fig. 4f), and enhanced the light-evoked glutamatergic inward currents (Fig. 4c, summary in Fig. 4f). These findings indicate that the outward currents were mediated by GABA transmission. The short latency and low jitter of light-evoked currents (Supplementary Fig. 8a, b), together with the persistence of the light-evoked GABAergic outward current during NBQX application suggests that the GABAergic outward current is mediated by monosynaptic GABA release, rather than polysynaptic glutamate-driven GABA release. To test whether light stimulation of ChR2-eYFP mesohabenular terminals results in both monosynaptic inward currents and outward currents, LHb neurons from VGluT2-ChR2 mice or rats injected in VTA with a nonspecific CaMKIIα-ChR2-eYFP vector (CaMKIIα-ChR2 rats) were recorded with and without tetrodotoxin (TTX)[23–25]. We replicated the inward glutamatergic currents and outward GABAergic currents in both VGluT2-ChR2 mice and CaMKIIα-ChR2 rats in response to light stimulation of ChR2-eYFP fibers in the absence of TTX (Supplementary Fig. 8c). TTX eliminated both inward and outward light-evoked currents, and both inward and outward light-evoked currents were recovered by blocking the delayed rectifier potassium channel with 4-aminopyridine (Supplementary Fig. 8c,d). Thus, both glutamate and GABA are released monosynaptically from mesohabenular axon terminals.

To confirm glutamatergic and GABAergic co-transmission by mesohabenular terminals from VTA dual $VGluT2^+$ $GABA^+$ neurons, we next performed intracellular recordings from individual LHb neurons in brain slices obtained from mice expressing ChR2-eYFP under the control of the VGaT promoter (VGaT-ChR2 mice; Fig. 4g). Similar to results obtained with VGluT2-ChR2 mice, light stimulation of VGaT-ChR2 mesohabenular fibers evoked inward currents that were blocked by NBQX (1 μM) without affecting the light-evoked outward currents (Fig. 4h). Furthermore, in the same LHb neurons, light-evoked outward currents were also blocked by picrotoxin (50 μM) (Fig. 4h). Thus, utilizing two transgenic mouse lines we demonstrate that in the adult rodent brain the mesohabenular terminals from VTA co-transmit glutamate and GABA onto LHb neurons. Although this type of co-transmission has been postulated to occur within the central nervous system in adulthood[26], these results provide the first direct evidence for such a synaptic response.

## Firing patterns evoked by mesohabenular activation *in vivo*

To determine the net effect of mesohabenular currents upon LHb firing patterns, we recorded from spontaneously active LHb neurons in urethane-anesthetized mice (VGluT2-ChR2 mice and VGaT-ChR2 mice; Fig. 5a) and in CaMKIIα-ChR2 rats (Fig. 5b). In order to mimic the

burst firing output of non-dopaminergic VTA neurons in response to rewarding or aversive events[27–28], mesohabenular fibers were optically stimulated using parameters that evoked burst firing in VGluT2 VTA neurons (10 ms pulses of 473 nm light presented every two seconds; Supplementary Fig. 9). This stimulation evoked inhibitory or excitatory firing patterns in LHb neurons, characterized as follows: (1) a short latency decrease in firing rate followed by slow return to pre-stimulation firing rates (inhibition); (2) a short latency decrease in firing rate followed by increased firing rates (inhibition-excitation); (3) a short latency increase in firing rate (excitation) or (4) a short latency increase in firing rate followed by decreased firing rates (excitation-inhibition) (Fig. 5c). Approximately 70% of LHb neurons were initially inhibited and 30% were initially excited by single brief light stimulation of mesohabenular fibers, and this was independent of either rodent species or ChR2 promoter (Fig. 5d–f; 38/54 LHb neurons from 13 VGluT2-ChR2 mice; 11/13 LHb neurons from 4 VGaT-ChR2 mice and 16/21 LHb neurons from 7 CaMKIIα-ChR2 rats). The inhibited and excited LHb neurons were broadly distributed throughout the LHb (Supplementary Fig. 10). The light-evoked inhibition of LHb neurons in VGluT2-ChR2 mice was significantly reduced by local application of the $GABA_A$-receptor antagonists bicuculline (20.7 ± 6.3% of baseline firing rate prior to bicuculline application versus 93.7 ± 20.3% of baseline firing rate following bicuculline application) or picrotoxin (20.9 ± 4.8% of baseline firing rate prior to picrotoxin application versus 70.8 ± 16.4% of baseline firing rate following picrotoxin application; Fig. 6). Though $GABA_A$ receptor antagonists can act upon small conductance potassium channels[29], the picrotoxin- and bicuculline-sensitivity of mesohabenular inhibition further supports the GABA release capabilities of VTA $VGluT2^+$ $GABA^+$ projections to LHb.

We next examined the light-evoked excitation of LHb neurons in VGluT2-ChR2 mice. Two different components of the excitation were uncovered by the intra-LHb administration of a cocktail of AMPA and NMDA receptor antagonists (CNQX and AP5): an early excitation sensitive to CNQX-AP5 (mean ± s.e.m. response magnitude 73.1 ± 14.3 spikes during baseline and 28.2 ± 3.7 spikes following CNQX-AP5 administration, Fig. 7), and a delayed excitation insensitive to CNQX-AP5 (Fig. 7a–d). These findings demonstrate that stimulation of mesohabenular $VGluT2^+$ $GABA^+$ fibers is capable of increasing the spiking activity of LHb neurons by glutamate release and that some of the excitation is independent of glutamate receptor activation. In conclusion, the molecular and synaptic architecture of the $VGluT2^+$ $GABA^+$ mesohabenular projection is organized to integrate signals that result in complex functional changes in LHb neurons.

## Discussion

We demonstrate using both anatomical and electrophysiological approaches that the major ascending projection from VTA to LHb arises from a newly identified phenotype of neurons that co-express VGluT2 and GAD mRNA. VGluT2-expressing VTA neurons are known to be highly heterogeneous[30] and the discovery of the VTA $VGluT2^+$ $GABA^+$ neurons herein provides further evidence that glutamatergic VTA neurons participate in diverse functions. Within the LHb, single axon terminals from these $VGluT2^+$ $GABA^+$ neurons express vesicular transporters responsible for accumulating both glutamate (via VGluT2) and GABA (via VGaT). Postsynaptic to a single mesohabenular axon terminal are both $GABA_A$

receptors and GluR1 receptors. Consistent with these anatomical findings, selective activation of mesohabenular terminals evokes both monosynaptic glutamate receptor- and GABA receptor-mediated currents in LHb neurons, and results in both inhibition and excitation of LHb neurons *in vivo*.

## Co-transmission of glutamate and GABA from VTA to LHb

Co-transmission of glutamate and GABA extends previous findings demonstrating co-transmission of glutamate and dopamine, or GABA and dopamine, from VTA neurons[25,31–33]. Because LHb appears to lack local inhibitory circuitry[34], we hypothesize that co-transmission of GABA and glutamate from mesohabenular axons may in some cases facilitate the shunting of excitatory currents, thereby balancing excitation and inhibition. Co-transmission of glutamate and GABA from VTA to LHb is likely a consequence of their unique synaptic architecture, which we have shown here to be a surprisingly common type of synaptic structure in the LHb. We found that the majority of LHb axon terminals co-express VGluT2 and VGaT, and that more than three quarters of the GABA axon terminals co-express VGluT2. Thus, the LHb is the first recognized brain structure in which the majority of GABAergic inputs are also glutamatergic. The present data indicate that the VTA is a major source of these glutamate-GABA inputs to LHb. The mesohabenular axon terminals expressing both VGluT2 and VGaT that simultaneously establish asymmetric (associated with synaptic excitation[19]) and symmetric (associated with synaptic inhibition[19]) synapses represents a newly identified synaptic arrangement.

Consistent with dual asymmetric and symmetric synapses from a single mesohabenular glutamatergic/GABAergic axon terminal, *in vivo* activation of these axon terminals evokes either fast inhibition that may be followed by excitation, or fast excitation that may be followed by inhibition. LHb neurons postsynaptic to mesohabenular axon terminals showed co-expression of $GABA_A$ receptors and GluR1-containing AMPA receptors, which are likely to contribute to the detected multimodal responses of LHb neurons after activation of mesohabenular terminals. The multimodal responses of LHb neurons may reflect differential activation of postsynaptic LHb glutamate or GABA receptors following release of glutamate and GABA from the same mesohabenular axon terminal. In addition, the degree of shunting of glutamatergic responses by the concurrent release of GABA may depend upon the activity pattern or resting membrane potential of individual postsynaptic LHb neurons. Regardless of the mechanism, our findings demonstrate that while glutamate release consistently resulted in increased LHb firing rates, GABA release resulted in either inhibitory firing alone or initial inhibition followed by a rebound excitatory firing, suggesting that a major function of the mesohabenular pathway is to provide a temporally-controlled change in LHb neuron firing rates.

## Potential implications

The timescale of changes in firing rate in LHb neurons evoked by activation of mesohabenular terminals is similar to the timescale of changes in firing rate by LHb neurons and non-dopaminergic VTA neurons in response to rewards, punishers, their predictors, and other salient stimuli[1, 3–4, 8, 27–28], suggesting a role for mesohabenular neurons in these processes. Moreover, rodent models of depression and addiction have shown alterations in

the molecular composition of LHb glutamate and GABA receptors[5,35] which are both postsynaptic to single mesohabenular axon terminals, raising the possibility that mesohabenular system plays a role in these pathologies. Considering the complexity of depression and addiction, disorders involving VTA and LHb dysfunction[2, 5, 7, 36–39], the discovery of a single anatomically-defined pathway capable of exciting or inhibiting LHb neurons provides novel insight into the interactions of brain regions responsible for these disorders.

## Online Methods

A supplementary methods checklist is available.

### Animals and Surgical Procedures

All animal procedures were performed in accordance with NIH Guidelines, and approved by the NIDA Animal Care and Use Committee

**Retrograde tracer injections—**Male Sprague Dawley (SD) rats (10–15 weeks; 400–450 g) were anesthetized with Equithesin (3.3 ml/kg, i.p.) in a physiological saline solution. FluoroGold (FG; 1% in cacodylate buffer, pH 7.5) was delivered unilaterally into the lateral habenula (LHb) [−3.4 mm anteroposterior (AP), 0.9 mm mediolateral (ML), and 5.4 mm dorsoventral (DV) from skull]iontophoretically through a stereotaxically positioned glass micropipette (inner tip diameter between 18–36 μm) by applying 1 μA current in 5 s pulses at 10 s intervals for 15 min. After each injection, the micropipette was left in place for an additional 10 min to prevent backflow. Following surgery, rats were single housed with a reversed 12:12 light/dark cycle, and perfused a week later.

**Virus injections—**Male VGluT2-IRES::Cre (*Slc17a6*$^{tm2(cre)Lowl}$/J) or VGaT-IRES::Cre (*Slc32a1*$^{tm2(cre)Lowl}$/Jmice (6–12 weeks;20–30g) (both in C57BL/6J background from The Jackson Laboratories, Bar Harbor, ME), and male SD rats (5–10 weeks;260–280g; Harlan) were anesthetized with 1–5% isofluorane. Cre-dependent AAV1-EF1α-DIO-ChR2-eYFP (for electrophysiology) or AAV5-EF1α-DIO-ChR2-mCherry (for microscopy) was injected in the ventral tegmental area (VTA) of mice (350 nL, 100 nL/min, −3.2 mm AP, 0.0 mm ML, −4.3 mm DV from skull for electrophysiology; 200 nL, 100 nL/min, −3.4 mm AP, ±0.2 mm ML, −4.3 mm DV from skull for microscopy). Rats were injected in VTA with AAV1-CaMKIIα-ChR2-eYFP (500 nL, 100 nL/min, −5.4 mm AP, −2.0 mm ML at 10°, −8.0 mm DV from skull). The CaMKIIα virus was chosen to infect all types of VTA neurons. Injections were made using the UltraMicroPump with Micro 4 controller, 10 uL Nanofil syringes, and 35 gauge needles (WPI Inc, Sarasota, FL). Syringes were left in place for 10 min following injections to minimize diffusion. Following surgery, mice were housed in 1–5 pairs, and rats were single housed, with a reversed 12:12 light/dark cycle. Six week after viral injections, animals were perfused or used for recordings.

### Retrograde tract tracing and in situ hybridization

**Tissue preparation—**Rats were anesthetized with chloral hydrate (0.5 ml/kg) and perfused transcardially with 4% (w/v) paraformaldehyde (PF) in 0.1 M phosphate buffer

(PB), pH 7.3. Brains were left in 4% PF for 2 h and transferred to 18% sucrose in PB overnight at 4°C. Coronal serial cryo-sections of VTA (16 μm) and LHb (30 μm) were prepared.

**Phenotyping of retrogradely labeled cells by immunocytochemistry and in situ hybridization—**FG labeled neurons were immunolabeled as we previously detailed[18]. Midbrain sections were incubated for 2 h at 30°C with rabbit anti-FG antibody (1:500; AB153; Millipore) and mouse anti-TH antibody (1:500; MAB318, Millipore). We had previously demonstrated specificity of primary antibodies[40,41]. Sections incubated in biotinylated goat anti-rabbit antibody (1:200; BA1000, Vector Laboratories, Burlingame CA) and fluorescein-conjugated donkey anti-mouse antibody (1:50; 715-095-151, Jackson ImmunoResearch, West Grove PA) for 1 h at30°C. Sections were kept in rinsed 4% PF while sections were imaged. After image collection, sections were processed by single situ hybridization (for radioactive detection of VGluT2 mRNA or GAD65/67 mRNA) or double in situ hybridization (for radioactive detection of VGluT2 mRNA and non-radioactive detection for transcripts encoding the two isoforms of glutamic acid decarboxylase; GAD65/67 mRNA) as previously detailed[40]. For single in situ hybridization, sections were hybridized for 16 h at 55°C with [$^{35}$S]- and [$^{33}$P]-labeled single-stranded antisense of either VGluT2 (nucleotides 317–2357; GenBank accession number NM-053427) or GAD65 and GAD67 (nucleotides 1–1758, accession number NM012563 and nucleotides 1–1782, accession number NM017007) probes at $10^7$cpm/ml. For double in situ hybridization, sections were incubated with [$^{35}$S]- and [$^{33}$P]-labeled single-stranded antisense of VGluT2 together with the single-stranded rat digoxigenin (DIG)-labeled antisense GAD65 and GAD67. To develop DIG signal, sections were incubated with an alkaline phosphatase-conjugated antibody against DIG (Roache Applied Science; Indianapolis, IN) for 3 hours at room temperature (RT); alkaline phosphatase reaction was developed with nitroblue tetrazolium and 5-bromo-4-chloro-3-indolyl phosphate (Life Technologies; Gaithersburg, MD) yielding a purple reaction product. Sections were then photographed under brightfield illumination. All sections were rinsed with PB and incubated for 1 h at RT in avidin-biotinylated horseradish peroxidase (1:200, ABC kit; Vector Laboratories). Sections were rinsed, and peroxidase reaction was developed with 0.05% 3, 3-diaminobenzidine-4 HCl (DAB) and 0.03% hydrogen peroxide ($H_2O_2$). Sections were mounted on coated slides. Slides were dipped in Ilford K.5 nuclear tract emulsion (Polysciences; 1:1 dilution in double distilled water) and exposed in the dark at 4°C for 3–4 weeks before development.

**Data analysis of in situ hybridization studies—**Sections were viewed, analyzed, and photographed with bright-field or epiluminescence microscopy using an Olympus BX51 microscope. Neurons were observed within each traced region at high power (20× or 40× objective lenses) and marked electronically. Subdivisions of the VTA were traced according to previously described methods[18]. FG-VGluT2, FG-GAD, and FG-VGluT2-GAD labeled material was analyzed using epiluminescence to increase the contrast of silver grains, identical to previous reports from our laboratory[18,33,40]. For VGluT2 *in situ* hybridization procedures, FG fluorescent cells containing or lacking TH fluorescent signal were photographed before processing for *in situ* hybridization. For all radioactive *in situ* hybridization methods (VGluT2 mRNA or GAD65/67 mRNA), a cell was considered to

express transcripts when its soma contained concentric aggregates of silver grains above background level. FG-labeled cells expressing VGluT2 or GAD65/67 mRNA, GAD65/67 mRNA and TH were counted separately. FG (brown DAB labeled) and radioactive *in situ* hybridization (silver grains) double-labeled material was analyzed by the following procedure: (1) silver grains corresponding to VGluT2 or GAD65/67 mRNA expression were focused under epiluminescence microscopy, (2) the path of epiluminescence light was blocked without changing the focus, and (3) bright-field light was used to determine whether a brown neuron, expressing FG in focus, contained the aggregates of silver grains seen under epiluminescence. FG (brown DAB product), nonradioactive GAD65/67 *in situ* hybridization (DIG probe labeled in purple), and radioactive VGluT2 *in situ* hybridization (silver grain) triple-labeled material was analyzed by the same procedure but in addition, cells were considered to express DIG-labeled transcripts (GAD mRNA) when its soma was the same shape as DAB-labeled FG cells. Neurons were counted when the stained cell was at least 5 μm in diameter. Pictures were adjusted to match contrast and brightness by using Adobe Photoshop (Adobe Systems). Cell counting was completed blind of injection site by three scorers and the inter rater reliability was 95.6%. Any FG-labeled neuron localized external to the VTA was excluded from analysis. Number of analyzed rats was based on previous studies in our lab using radioactive detection of VGluT2 mRNA from rat VTA neurons[18,33,40].

## Confocal and electron microscopy

VGluT2-IRES::Cre mice were anesthetized with chloral hydrate (35 mg/100 g) and perfused transcardially with a fixative solution containing 4% PF with 0.15% glutaraldehyde and 15% picric acid in 0.1 M in 0.1 M PB, pH 7.3. Brains were left in this fixative solution for 2 h at 4°C, solution was replaced with 2% PF and left overnight at 4°C. Brains were rinsed with PB cut into coronal serial sections (50 μm thick) with a vibratome (VT1000S, Leica, Vienna, Austria).

**Immunolabeling for Light Microscopy—**To determine whether the injected transduced virus was confined to VTA neurons and reporter gene mCherry expressed in the LHb, every fifth section of the VTA or LHb was used to detect mCherry by immunohistochemistry. Sections were incubated with a blocking solution [4% bovine serum albumin (BSA) in PB supplemented with 0.3% Triton-X-100] for 1 h. Sections were then incubated with mouse anti-mCherry antibody (632543; Clontech Laboratories Inc., Mountain View, CA, 1:500 dilution) in the blocking solution overnight at 4°C. After PB rinsing, sections were incubated for 1h at RT with biotinylated goat anti-mouse secondary antibody, rinsed with PB, and incubated with avidin-biotinylated horseradish peroxidase for 1h. Sections were rinsed and the peroxidase reaction was then developed with 0.05% DAB and 0.003% $H_2O_2$. The specificity of primary anti-mCherry antibodies was demonstrated by the lack mCherry immunolabeling in brain sections from mice injected with saline solution without mCherry.

**Fluorescence Microscopy and Three-dimensional Analysis—**Coronal LHb sections were incubated for 1 h in PB supplemented with 4% BSA and 0.3% Triton X-100. Sections were then incubated with a cocktail of mouse anti-mCherry antibody, guinea pig anti-VGluT2 antibody (VGluT2-GP-Af240-1; Frontier Institute Co., Ltd, Japan, 1:500), and

rabbit anti-VGaT antibody (VGAT-Rb-Af500; Frontier Institute Co., Ltd, 1:500), or a cocktail of mouse anti-mCherry antibody, guinea pig anti-$GABA_A$ receptor antibody (GABAARa1-GP-Af440; Frontier Institute Co. Ltd, Japan, 1:200 dilution), rabbit anti-GluR1 antibody (GluR1C-Rb-Af692-1; Frontier Institute Co. Ltd, Japan, 1:200 dilution) overnight at 4°C. Specificity of primary antibodies has been previous shown[42–44]. After PB rinsing, sections were incubated in a cocktail of fluorescent donkey secondary antibodies (Jackson Immunoresearch Laboratories Inc., 1:100); Alexa Fluor 488 anti-guinea pig (706-545-14), Alexa Fluor 594 anti-mouse (715-585-151) and Alexa Fluor 647 anti-rabbit (711-605-152), or in a cocktail of Alexa Fluor 488 anti-rabbit (711-545-152), Alexa Fluor 594 anti-mouse (715-585-151), and Alexa Fluor 647 anti-guinea pig (706-585-148). After rinsing, sections were mounted with Vectashield mounting medium (H1000; Vector Laboratories) on slides and air-dried. Fluorescent images were collected with Olympus FV1000 Confocal System (Olympus, Center Valley, PA). Images were taken sequentially with different lasers with 100× oil immersion objectives and z-axis stacks were collected at intervals of 0.1 μm. Imaris microscopy software (Bitplane Inc., South Windsor, CT) was used to analyze z-stacks of confocal images from 3 mice (62 × 62 × 5 μm for each image, 4 images from each mouse between bregma −1.22 mm to −2.18 mm) to obtain three-dimensional quantification of axon terminals expressing mCherry, VGluT2 or VGaT. The same confocal images were analyzed with the Amira microscopy software (Visualization Sciences Group, Burlington, MA) to obtain three-dimensional reconstruction of axon terminals. Using these software, quantification occurred blindly. Differences in numbers of $VGluT2^+$ $VGaT^+$, $VGluT2^+$ $VGaT^-$, and $VGluT2^-$ $VGaT^+$ mesohabenular terminals were analyzed in GraphPad prism 5. We analyzed over 2000 mesohabenular axon terminal samples from three mice, which provided statistical power to detect small effects. Since the data distribution was skewed, we used the nonparametric Friedman test to analyze differences between the three mesohabenular axon terminal phenotypes. Posthoc Dunn's multiple comparison tests were used to analyze differences between specific axon terminal phenotypes.

**Electron Microscopy—**Coronal LHb sections were rinsed with 0.1 M PB (pH 7.3), incubated with 1% sodium borohydride in PB for 30 min, rinsed in PB, and then incubated with blocking solution [1% normal goat serum (NGS), 4% BSA in PB supplemented with 0.02% saponin] for 30 min. Sections were incubated with cocktail of primary antibodies: mouse anti-mCherry + guinea pig anti-VGluT2 (1:400), mouse anti-mCherry (1:1000) + rabbit anti-VGaT (1:400), mouse anti-mCherry + rabbit anti-GluR1 (1:200), mouse anti-mCherry + guinea pig anti-$GABA_A$ receptor (1:200), rabbit anti-GluR1 + anti-$GABA_A$ receptor, guinea pig anti-VGluT2 + rabbit-anti-VGaT, guinea pig anti-VGluT2, or rabbit anti-VGaT. All primary antibodies were diluted in PB with 1% NGS and incubations were for 24 h at 4°C. All gold-coupled secondary antibodies (Nanoprobes Inc., Stony Brook, NY) were couple to 1.4 nm gold and used at 1:100 dilution. Sections were rinsed and incubated overnight at 4°C in the corresponding secondary antibodies: biotinylated goat anti-mouse antibody (for mCherry detection) + anti-guinea pig IgG Fab' fragment gold-coupled (catalog number 205; for VGluT2 detection) or biotinylated goat anti-mouse antibody (for mCherry detection) + anti-rabbit IgG gold-coupled (catalog number 2003; for VGaT detection), biotinylated goat anti-mouse antibody (for mCherry detection) + anti-rabbit IgG gold-

coupled (for GluR1 detection), biotinylated goat anti-mouse antibody (for mCherry detection) + anti-guinea pig IgG Fab' fragment gold-coupled (for $GABA_A$ receptor detection), biotinylated goat anti-rabbit antibody (for GluR1 detection) + anti-guinea pig IgG Fab' fragment gold-coupled (for $GABA_A$ receptor detection), biotinylated goat anti guinea pig antibody (for $GABA_A$ receptor detection) + anti-rabbit IgG gold-coupled (for GluR1 detection), biotinylated goat anti-rabbit antibody (for VGaT detection) + anti-guinea pig IgG Fab' fragment gold-coupled (for VGluT2 detection), biotinylated goat anti guinea pig antibody (for VGluT2 detection) + anti-rabbit IgG gold-coupled (for VGaT detection), anti-guinea pig IgG Fab' fragment gold-coupled (for VGluT2 detection), or anti-rabbit IgG gold-coupled (for VGaT detection). Silver enhancement of the gold particles was done using the Nanoprobe Silver Kit (2012; Nanoprobes Inc.). Then, sections were incubated in avidin-biotinylated horseradish peroxidase complex (1:100 dilution) in PB for 2 h at RT and incubated with 0.025% DAB and 0.003% $H_2O_2$ in PB. Sections were fixed with 0.5% osmium tetroxide in PB for 25 min, and contrasted in1% uranyl acetate for 35 min. Sections were dehydrated and resin embedded, and ultrathin section prepared as we previously detailed[45]. Sections were examined and photographed using a Tecnai G2 12 transmission electron microscope (FEI Company, Hillsboro, OR) equipped with a digital micrograph 3.4 camera (Gatan, Inc., Pleasanton, CA).

**Ultrastructural Analysis—**Serial thin sections of LHb (bregma −1.22 mm to −2.18 mm) were analyzed. Synaptic contacts were classified according to their morphology and immunolabeling, and photographed at a magnification of 6,800–13,000X. The morphological criteria used for identification and classification of cellular components observed in these thin sections were as previously described[19,20]. Type I synapses, referred to here as asymmetric synapses, were defined by the presence of contiguous synaptic vesicles within the presynaptic axon terminal and a thick postsynaptic density (PSD) greater than 40 nm[20]. Type II synapses, referred to here as symmetric synapses, were defined by the presence of contiguous synaptic vesicles within the presynaptic axon terminal and a thin PSD[20]. Puncta adhaerentia, mechanical adhesion sites between presynaptic and postsynaptic sites were defined by the absence of synaptic vesicles within the presynaptic axon terminal and a PSD[20]. Serial sections were obtained to confirm the type of synapse. In the serial section analyses of VGluT2 and VGaT expression, a terminal containing greater than 5 immunogold particles was considered an immunogold-positive terminal. Pictures were adjusted to match contrast and brightness by using Adobe Photoshop (Adobe Systems Incorporated, Seattle, WA). Data collection and analysis were performed blind to the conditions of the experiments.

## Whole cell recordings of LHb neurons

**Slice preparation—**Male VGluT2-ChR2mice (n = 8), VGaT-ChR2 mice (n = 3), and CaMKIIα-ChR2 rats (n = 3) were euthanized by isofluorane followed by rapid decapitation. The brains were then removed and placed into a chilled (4°C) and aerated (95% $O_2$/5% $CO_2$) modified artificial cerebrospinal fluid comprised of (mM): NaCl, 87; KCl, 2.5; $MgCl_2$, 7; $CaCl_2$, 0.5; $NaH_2PO_4$, 1.25; d-glucose, 25; sucrose, 75; $NaHCO_3$, 25. Coronal slices containing the LHb were cut (280 μm) using a vibrotome. Slices were transferred to a holding chamber containing normal aCSF consisting of (mM): NaCl, 126; KCl, 3.0; $MgCl_2$,

1.5; $CaCl_2$, 2.4; $NaH_2PO_4$, 1.2; glucose, 11.0; $NaHCO_3$, 26, saturated with 95% $O_2$/5% $CO_2$, at 35°C for 20–25 min and subsequently maintained at RT for ≥1 h prior to recordings.

**Intracellular recordings—**Slices were submerged in a low-volume (~170 μl) recording chamber (RC-22; Warner Instruments, Hamden, CT) and continuously superfused at 2ml/min with warm (30–32°C) aCSF containing 40μM D-(−)-2-Amino-5-phosphonopentanoic acid (D-APV) to block NMDA receptors (control medium). Visualization of LHb neurons was performed using an upright microscope equipped with epifluorescence and differential interference contrast-infrared microscopy (Axioskop-2, Carl Zeiss). Recording electrodes (3–5 MΩ) were filled with an intracellular solution consisting of (in mM): K-gluconate, 140; KCl, 5; HEPES, 10; EGTA, 0.2; $MgCl_2$, 2; Mg-ATP, 4; $Na_2$-GTP, 0.3; $Na_2$-phosphocreatine, 10; pH 7.2. The intracellular solution also contained 0.2% biocytin. Neurons were sampled randomly from the LHb. Whole-cell voltage clamp recordings were performed using a Multiclamp 700B (Molecular Devices, Sunnyvale, CA). Data acquisition was performed using WinLTP (WinLTP Ltd, Bristol, UK) and an A/D board (National Instruments PCI-6251). Optical stimulation was delivered to the slice via an optical fiber (200 μm core, Thorlabs, Newton, NJ) coupled to a 150 mW, 473 nm diode pumped solid state continuous wave laser system (OEM Laser Systems Salt Lake City, UT). Stimulation consisted of either a single 5 ms pulse, or paired 5 ms pulses delivered 50 ms apart. Output of the laser was <2 mW. Light-evoked responses and the effects of AMPA-receptor antagonist (NBQX) or GABA (picrotoxin) antagonists on these responses were recorded over several holding potentials (between −45 mV and −80 mV). Order of presentation of NBQX and picrotoxin was counterbalanced and randomly assigned. All drugs were dissolved in aCSF. Paired t-tests compared the average light-evoked response in control medium to the minimum light-evoked response (peak drug effect) in drug medium. Light-evoked changes were predicted to either have no change or be abolished by drug application. The expected standard deviation of pre vs. post drug effects used in power calculations was 40, based on analysis of previous results. Using this criteria, a minimum of four pairs of neurons receiving both pre and post drug examination provided adequate power to detect large effects.

To evaluate monosynaptic transmission from VTA to LHb, whole cell recordings of LHb neurons were performed under conditions described above without AMPA receptor or $GABA_A$ receptor antagonists. Light-evoked responses were recorded at −50 mV and −70 mV holding potentials in control medium, and subsequently in the presence of TTX (1 μM),followed by TTX with 4-AP (200 μM). Latency was calculated from the onset of the light pulse to 10% of the peak response. Jitter was calculated as the standard deviation of the latency measured from 8–10 responses[46]. A two-way repeated measures ANOVA was used to test for significant differences in percent of light evoked current from control conditions within rodent (CaMKIIα-ChR2 rats or VGluT2-ChR2 mice) and TTX condition (TTX or TTX/4AP). Sidak adjusted pairwise comparisons were used to examine differences between TTX conditions within each rodent species. Data collection and analysis were not performed blind to the conditions of the experiments. Following intracellular recordings, slices were stored in a 4% PF solution overnight at 4°C, rinsed with PB and incubated in Alexa Fluor 546 streptavidin (1:500, Invitrogen) for 2 h at RT.

### In vivo single-unit recordings of LHb and VTA neurons

**In vivo recordings—**Male VGluT2-ChR2 mice (n = 32), VGaT-ChR2 mice (n = 5), and CaMKIIα-ChR2 rats (n = 9) were anesthetized with urethane (1.4 g/kg, IP), and mounted in a stereotaxic frame. A hole was drilled in the skull to access the LHb or VTA. Glass micropipettes (6–10 MΩ) filled with 2.0% Pontamine Sky Blue (BDH Chemicals, Poole, England) in 3M NaCl were used for recordings. Glass electrodes were utilized to shield against any potential light-induced artifacts that can be observed with metal electrode recordings alone[47]. A 100 μm core multimode fiber was glued 350 μm dorsal to the glass electrode tip, and the fiber was connected to a 473 nm DPSS laser (OEM laser systems, Bluffdale, UT). Signals were amplified using a Neuro Data IR283A (Cygnus Technology, Delaware Water Gap, PA) and BrownLee 440 amplifier. Neuronal activity was bandpass filtered between 300 Hz and 3000 Hz. The biopotentials were digitized using a Power 1401 Analogue-Digital Converter (Cambridge Electronic Design, Cambridge UK). Spontaneously active oroptogenetically-driven neurons were recorded and analyzed. LHb recordings were obtained from rats between −3.0 to −3.8 mm AP, 0.5 to 1.0 mm ML, and −4.3 to −5.4 DV and from mice between −1.2 to 2.0 mm AP, 0.2 to 0.6 mm ML and −2.9 to −3.6 mm DV. Entrance into the LHb was demarcated by passage through the hippocampus. Immediately following the hippocampus a rise in background noise was observed through the ventricle, after which background noise subsided and neurons were recorded within the LHb with electrophysiological properties as previous reports[34]. VTA recordings were obtained from VGluT2-IRES::Cre mice between −3.1 to −3.5 mm AP, 0 to 0.5 mm ML and −4.2 to −4.6 mm DV. Entrance into the VTA was demarked by passage through a layer of fast firing neurons dorsal to the VTA. Neurons were randomly sampled by slowly lowering the micropipette through the LHb or VTA while 10 ms pulses of 473 nm light (20 mW) every 2 sec were applied. After encountering a neuron, baseline activity was recorded for 2 to 5 min, peristimulus time histograms were constructed at 5 ms resolution bins, with a window width of 0.5 s before and 1 s after the stimulus onset. Fidelity was defined as the percent of occasions in which laser stimulation evoked spiking in the recorded neuron. Signal to noise ratio was typically >5:1. After recordings, animals were perfused with 4% PF, LHb and VTA cryosections (30 μm) were prepared to verify the deposit of the pontamine sky in the recording sites, and expression of eYFP by immunostained with a mouse anti-GFP antibody (1:400, JL-8, Clontech, Mountain View, CA), as described for mCherry detection. Neurons recorded external to the LHb or VTA were excluded from the analysis. The specificity of primary anti-GFP antibodies was demonstrated by the lack GFP immunolabeling in brain sections from mice injected with saline solution without GFP.

**Local drug infusion—**A double-barrel pipette was assembled for local microinjection of drug while simultaneously recording LHb neurons. The recording pipette was similar to the described above in-vivo recording section and protruded approximately 130 μm beyond the injection tip (25–30 μm internal diameter). A 100 μm diameter optic fiber was glued 350 μm dorsal to the electrode tip. The injection pipette was filled with 50 nM bicuculline, 500 nM picrotoxin, cocktail of 50 μM CNQX and 100 μM AP-5 or vehicle. All drugs were dissolved in aCSF. After isolating a single LHb neuron, spontaneous activity was recorded to establish baseline activity, followed 100–200 10 ms 473 nm light pulses at 20 mW to determine responses to optical activation of VTA fibers on LHb activity. After 5 min of baseline

activity, drug was delivered (50–200 nl) using brief pulses of pneumatic pressure (Picospritzer, General Valve, Fairfield NJ), and the drug-effects were assessed every 10 min.

**Data Analysis—**For single 10 ms 473 nm light pulses, peristimulus time histograms (PSTHs) of 5 ms bin width of LHb or VTA activity were generated. PSTHs were analyzed to determine excitatory and inhibitory epochs. Mean and standard deviation of counts per bin were determined for a baseline period, defined as the 500 ms epoch preceding stimulation. The onset of excitation was defined as the first bin for which the mean value exceeded mean baseline activity by 2 standard deviations, and response offset was determined as the time at which activity had returned to be consistently within 2 standard deviations of baseline. Inhibition was defined as an epoch of at least 20 ms in which the mean count per bin was at least 30% less than that during baseline. Excitatory and inhibitory response magnitudes (R mags) were normalized for different levels of baseline impulse activity, allowing for comparison of drug effects on evoked responses independent of effects on baseline activity. R mags for excitation were calculated with the following equation: Excitation R mag = (counts in excitatory epoch) − (mean counts per baseline bin × number of bins in excitatory epoch). Some neurons exhibited a secondary response either excitation after inhibition or inhibition after excitation. Neurons were categorized by the first occurring response. We only analyzed the initial response that occurred after optical activation. Sample size was determined as described in the "Intracellular recordings" sections. Data collection and analysis were not performed blind to the conditions of the experiments.

**Statistics—**Parametric statistics were used after verifying compliance for normal distribution and equal variance assumptions. One-way and two-way ANOVA were used to compare between-groups effects. Repeated-measures ANOVAs were used to compare within-group effects across time. Normality was assessed using the D'Agostino and Pearson omnibus normality test. Equality of variance was assessed with the Bartlett's test for equal variances. The sphericity of the matrix assumption for repeated-measures ANOVA was assessed with the Mauchley Sphericity Test; when the outcome of the test was significant the F-values were corrected using the Greenhouse–Gaisser approach. Newman-Keuls post-hoc test was used to establish differences in means after the ANOVA. When requirement for parametric statistic were not met a Kruskal–Wallis' test was used to compare between-group differences.

## Supplementary Material

Refer to Web version on PubMed Central for supplementary material.

## Acknowledgments

The Intramural Research Program of the National Institute on Drug Abuse (IRP/NIDA/NIH) supported this work. We thank Drs. Roy Wise, Jia Qi, and Jose Aceves for their comments and JQ for assistance with viral injections used in ultrastructural experiments. Viruses were packaged by the NIDA IRP Optogenetics and Transgenic Technology Core.

## References


1. Matsumoto M, Hikosaka O. Lateral habenula as a source of negative reward signals in dopamine neurons. Nature. 2007; 447(7148):1111–1115. [PubMed: 17522629]
2. Friedman A, et al. Electrical stimulation of the lateral habenula produces enduring inhibitory effect on cocaine seeking behavior. Neuropharmacology. 2010; 59(6):452–459. [PubMed: 20600170]
3. Bromberg-Martin ES, et al. Distinct tonic and phasic anticipatory activity in lateral habenula and dopamine neurons. Neuron. 2010a; 67(1):144–155. [PubMed: 20624598]
4. Bromberg-Martin ES, Matsumoto M, Hong S, Hikosaka O. A pallidus-habenula-dopamine pathway signals inferred stimulus values. J Neurophysiol. 2010b; 104(2):1068–1076. [PubMed: 20538770]
5. Li B, et al. Synaptic potentiation onto habenula neurons in the learned helplessness model of depression. Nature. 2011; 470(7335):535–539. [PubMed: 21350486]
6. Jhou TC, et al. The rostromedial tegmental nucleus (RMTg), a GABAergic afferent to midbtain dopamine neurons, encodes aversive stimuli and inhibits motor responses. Neuron. 2009; 61:786–800. [PubMed: 19285474]
7. Jhou TC, et al. Cocaine drives aversive conditioning via delayed activation of dopamine-responsive habenular and midbrain pathways. J Neurosci. 2013; 33(17):7501–7512. [PubMed: 23616555]
8. Hong S, et al. Negative reward signals from the lateral habenula to dopamine neurons are mediated by rostromedial tegmental nucleus in primates. J Neurosci. 2011; 31(32):11457–11471. [PubMed: 21832176]
9. Stamatakis AM, Stuber GD. Activation of lateral habenula inputs to the ventral midbrain promotes behavioral avoidance. Nat Neurosci. 2012; 15(8):1105–1107. [PubMed: 22729176]
10. Lammel S, et al. Input-specific control of reward and aversion in the ventral tegmental area. Nature. 2012; 491(7423):212–217. [PubMed: 23064228]
11. Stamatakis AM, et al. A unique population of ventral tegmental area neurons inhibits the lateral habenula to promote reward. Neuron. 2013; 80(4):1039–1053. [PubMed: 24267654]
12. Swanson LW. The projections of the ventral tegmental area and adjacent regions: a combined fluorescent retrograde tracer and immunofluorescence study in the rat. Brain Res Bull. 1982; 9(1–6):321–353. [PubMed: 6816390]
13. Phillipson OT, Pycock CJ. Dopamine neurons of the ventral tegmentum project to both medial and lateral habenula. Some implications for Habenular function. Exp Br Res. 1982; 45:89–94.
14. Skagerberg G, Lindvall O, Björklund A. Origin, course and termination of the mesohabenular dopamine pathway in the rat. Brain Res. 1984; 307(1–2):99–108. [PubMed: 6087992]
15. Gruber C, et al. Dopaminergic projections from the VTA substantially contribute to the mesohabenular pathway in the rat. Neuroscience Letters. 2007; 427(3):165–170. [PubMed: 17949902]
16. Hnasko TS, et al. Ventral tegmental area glutamate neurons: electrophysiological properties and projections. J Neurosci. 2012; 32(43):15076–15085. [PubMed: 23100428]
17. Taylor SR, et al. GABAergic and glutamatergic efferents of the mouse ventral tegmental area. J Comp Neurol. 2014 in press.
18. Yamaguchi T, et al. Mesocorticolimbic glutamatergic pathway. J Neurosci. 2011; 31(23):8476–8490. [PubMed: 21653852]
19. Peters A, Palay SL. The morphology of synapses. J Neurocytol. 1996; 25:687–700. [PubMed: 9023718]
20. Peters, A.; Palay, S.; Webster, HDF. The Fine Structure of the Nervous System. New York, NY: Oxford University Press; 1991.
21. Boulland JL, et al. Vesicular glutamate and GABA transporters sort to distinct sets of vesicles in a population of presynaptic terminals. Cereb Cortex. 2009; 19(1):241–248. [PubMed: 18502731]
22. Foss SM, et al. Multiple dileucine-like motifs direct VGLUT1 trafficking. J Neurosci. 2013; 33:10647–10660. [PubMed: 23804088]
23. Petreanu L, Mao T, Sternson SM, Svoboda K. The subcellular organization of neocortical excitatory connections. Nature. 2009; 457(7233):1142–1145. [PubMed: 19151697]

24. Cruikshank SJ, Urabe H, Nurmikko AV, Connors BW. Pathway-specific feedforward circuits between thalamus and neocortex revealed by selective optical stimulation of axons. Neuron. 2010; 65(2):230–245. [PubMed: 20152129]
25. Tritsch NX, Ding JB, Sabatini BL. Dopaminergic neurons inhibit striatal output through non-canonical release of GABA. Nature. 2012; 490(7419):262–266. [PubMed: 23034651]
26. Münster-Wandowski A, Gómez-Lira G, Gutiérrez R. Mixed neurotransmission in the hippocampal mossy fibers. Front Cell Neurosci. 2013; 7 http://dx.doi.org/10.3389/fncel.2013.00210.
27. Cohen JY, et al. Neuron-type-specific signals for reward and punishment in the ventral tegmental area. Nature. 2012; 482(7383):85–88. [PubMed: 22258508]
28. Tan KR, et al. GABA neurons of the VTA drive conditioned place aversion. Neuron. 2012; 73(6): 1173–1183. [PubMed: 22445344]
29. Johnston GAR. Advantages of an antagonist: bicuculline and other GABA antagonists. Br J of Pharmacology. 2013; 169:328–336.
30. Morales M, Root DH. Glutamate neurons within the midbrain dopamine regions. Neuroscience. 2014 in press.
31. Sulzer D, et al. Dopamine neurons make glutamatergic synapses in vitro. J Neurosci. 1998; 18:4588–4602. [PubMed: 9614234]
32. Dal Bo G, et al. Dopamine neurons in culture express VGLUT2 explaining their capacity to release glutamate at synapses in addition to dopamine. J Neurochem. 2004; 88:1398–1405. [PubMed: 15009640]
33. Li X, et al. Heterogeneous composition of dopamine neurons of the rat A10 region: molecular evidence for diverse signaling properties. Brain Struct Funct. 2013; 218:1159–1176. [PubMed: 22926514]
34. Weiss T, Veh RW. Morphological and electrophysiological characteristics of neurons within identified subnuclei of the lateral habenula in rat brain slices. Neuroscience. 2011; 172:74–93. [PubMed: 20974229]
35. Maroteaux MM, Mameli M. Cocaine evokes projection-specific synaptic plasticity of lateral habenula neurons. J Neurosci. 2012; 32(36):12641–12646. [PubMed: 22956853]
36. Shabel SJ, et al. Input to the lateral habenula from the basal ganglia is excitatory, aversive, and suppressed by serotonin. Neuron. 2012; 74(3):475–481. [PubMed: 22578499]
37. Tye KM, et al. Dopamine neurons modulate neural encoding and expression of depression-related behaviour. Nature. 2013; 493(7433):537–541. [PubMed: 23235822]
38. Chaudhury D, et al. Rapid regulation of depression-related behaviours by control of midbrain dopamine neurons. Nature. 2013; 493(7433):532–536. [PubMed: 23235832]
39. Nair SG, Strand NS, Neumaier JF. DREAD Ding the lateral habenula: a review of methodological approaches for studying lateral habenula function. Brain Res. 2013; 1511:93–101. [PubMed: 23085473]
40. Yamaguchi T, Sheen W, Morales M. Glutamatergic neurons are present in the rat ventral tegmental area. Eur JNeurosci. 2007; 25:106–118. [PubMed: 17241272]
41. Tagliaferro P, Morales M. Synapses between corticotropin-releasing factor-containing axon terminals and dopaminergic neurons in the ventral tegmental area are predominantly glutamatergic. J Comp Neurol. 2008; 506:616–626. [PubMed: 18067140]
42. Miyazaki T, Fukaya M, Shimizu H, Watanabe M. Subtype switching of vesicular glutamate transporters at parallel fibre-Purkinjec cell synapses in developing mouse cerebellum. Eur J Neurosci. 2003; 17:2563–2573. [PubMed: 12823463]
43. Watanabe M, Fukaya M, Sakimura K, Manabe T, Mishina M, Inoue Y. Selective scarcity of NMDA receptor channel subunits in the stratum lucidum (mossy fibre-recipient layer) of the mouse hippocampal CA3 subfield. Eur J Neurosci. 1998; 10:478–487. [PubMed: 9749710]
44. Ichikawa R, et al. Developmental switching of perisomatic innervation from climbing fibers to basket cell fibers in cerebellar purkinje cells. J Neurosci. 2011; 31(47):16916–16927. [PubMed: 22114262]
45. Dobi A, Margolis EB, Wang HL, Harvey BK, Morales M. Glutamatergic and nonglutamatergic neurons of the ventral tegmental area establish local synaptic contacts with dopaminergic and nondopaminergic neurons. J Neurosci. 2010; 30:218–229. [PubMed: 20053904]

46. Pinol RA, Bateman R, Mendelowitz D. Optogenetic approaches to characterize the long-range synaptic pathways from the hypothalamus to brain stem autonomic nuclei. J Neurosci Methods. 2012; 210(2):238–246. [PubMed: 22890236]

47. Cardin JA, et al. Targeted optogenetic stimulation and recording of neurons in vivo using cell-type-specific expression of channelrhodopsin-2. Nat Protoc. 2010; 5(2):247–254. [PubMed: 20134425]

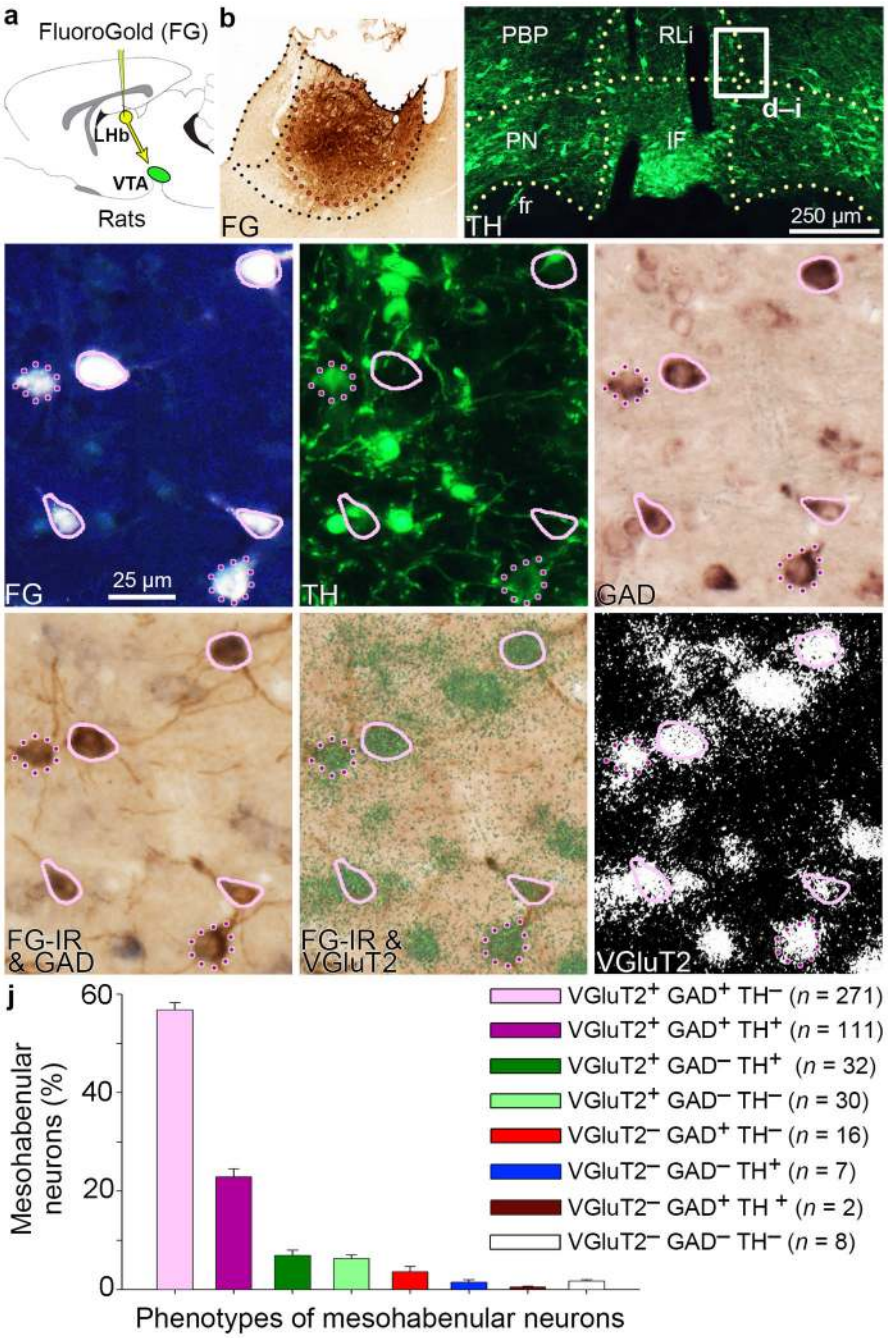


**Figure 1. Most VTA neurons projecting to LHb co-express VGluT2 and GAD**

(**a,b**) Delivery of the retrograde tracer FG into LHb. (**c**) FG-labeled VTA neurons were examined (TH; green). (**d–i**) Higher magnification of boxed area in **c**. FG is seen as white (**d**) or brown after its immunodetection (FG-IR; **g; h**). FG-labeled VTA neurons expressing TH (green cells; **e**), GAD65/67 mRNAs (purple cells; **f**) or VGluT2 mRNA (green-grain-aggregates, **h** or white-grains-aggregates, **i**). Most FG neurons co-expressed VGluT2 and GAD without TH (solid pink), fewer co-expressed TH (dotted purple). (**j**) Frequency of FG phenotypes (mean ± s.e.m.); 9–10 VTA sections each from three rats. RLi, rostral linear

nucleus; IF, interfascicular nucleus; PN, paranigral nucleus; PBP, parabrachial pigmentosis nucleus; fr, fasciculus retroflexus.

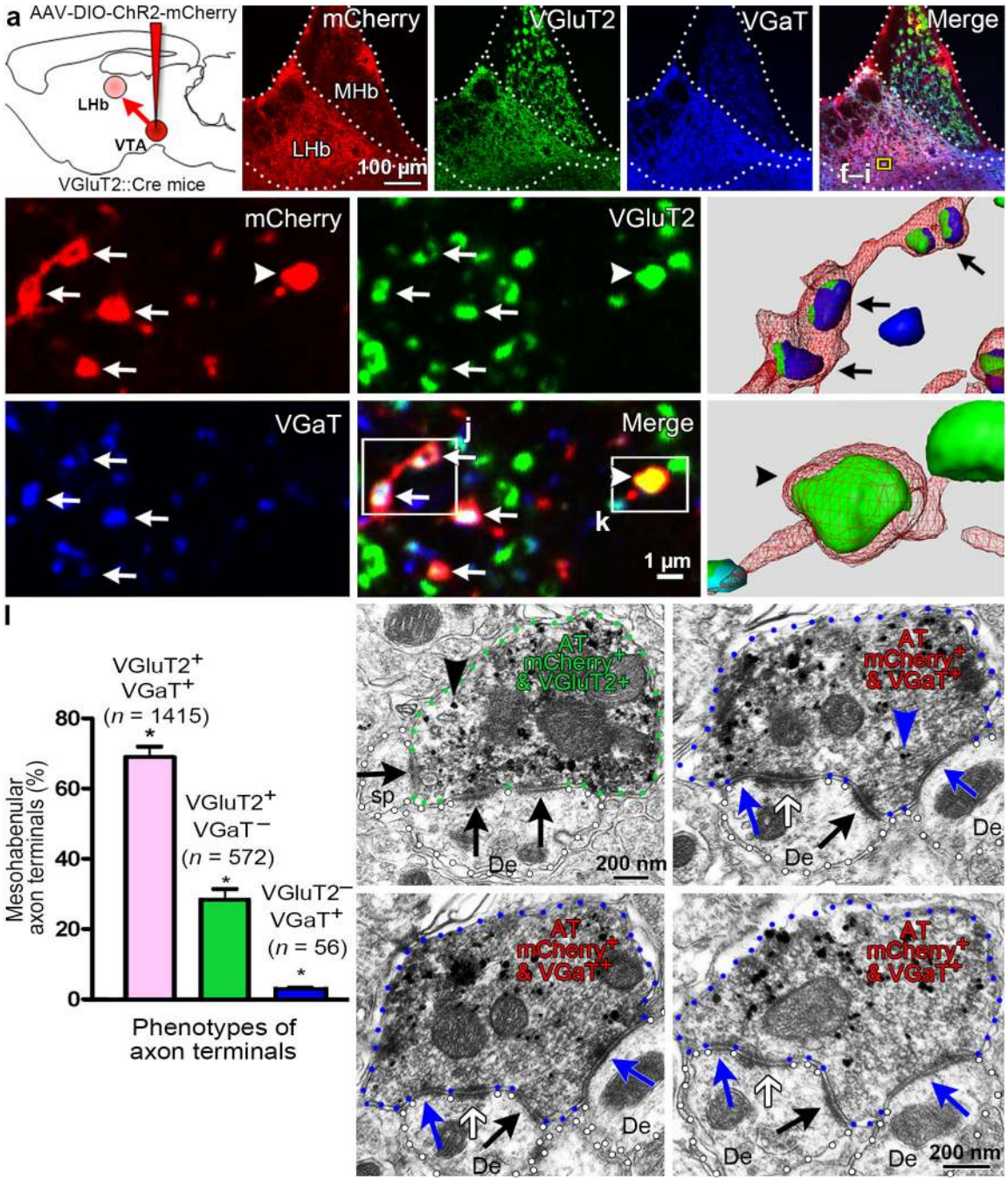


**Figure 2. Most mesohabenular axon terminals (AT) co-express VGluT2 and VGaT from which a single terminal simultaneously establishes symmetric and asymmetric synapses**

(**a**) Cre-inducible AAV-DIO-ChR2-mCherry vector injected into VTA of VGluT2::Cre mice. Mesohabenular AT were identified by mCherry expression and examined under confocal (**b–k**) or electron microscopy (**m–p**). (**b**) LHb, not medial habenula (MHb), was densely innervated by VTA-fibers (mCherry). Single focal planes showing immunolabeling for VGluT2 (**c**, green), VGaT (**d**, blue), and merge (**e**). (**f–i**) Higher magnification of e boxed area; arrows indicate mCherry AT (**f**) co-expressing VGluT2 (**g**) and VGaT (**h**), and

arrowheads indicate single VGluT2. (**i**) Merge. (**j,k**) 3-D reconstruction from boxed areas in i. (**l**) Frequency of AT-phenotypes (mean ± s.e.m.); 2043 mCherry AT were analyzed by 3-D reconstruction (12 LHb samples; 3 mice). Most AT co-expressed VGluT2 and VGaT, fewer had only VGluT2 or VGaT alone; significant AT phenotype effect by Friedman's test; $X^2(2) = 24$; p=0.000024; Dunn's multiple comparison test ($VGluT2^+VGaT^+$ versus $VGluT2^+VGaT^-$ rank sum difference = 12, p=0.0429; $VGluT2^+VGaT^+$ versus $VGluT2^-VGaT^+$ rank sum difference =24, $p < 0.0001$; $VGluT2^+VGaT^-$ versus $VGluT2^+VGaT^-$ rank sum difference = 12, p=0.0429; $^*p < 0.05$). (**m–p**) Sequential LHb sections from VGluT2-ChR2-mCherry mouse showing mCherry detection by immunoperoxidase-labeling (scattered dark material) and either VGluT2 (black arrowhead; **m**) or VGaT (blue arrowhead; **n**) detection by immunogold. Experiments were repeated successfully three times. (**m**) A mCherry-VGluT2 AT establishing asymmetric synapses (black arrows) with a dendrite (De) and dendritic spine (sp). (**n–p**) Serial sections of a mCherry-VGaT AT establishing with a De an asymmetric synapse (black arrow), a symmetric synapse (blue arrows) and a puncta adhaerentia (white arrow).

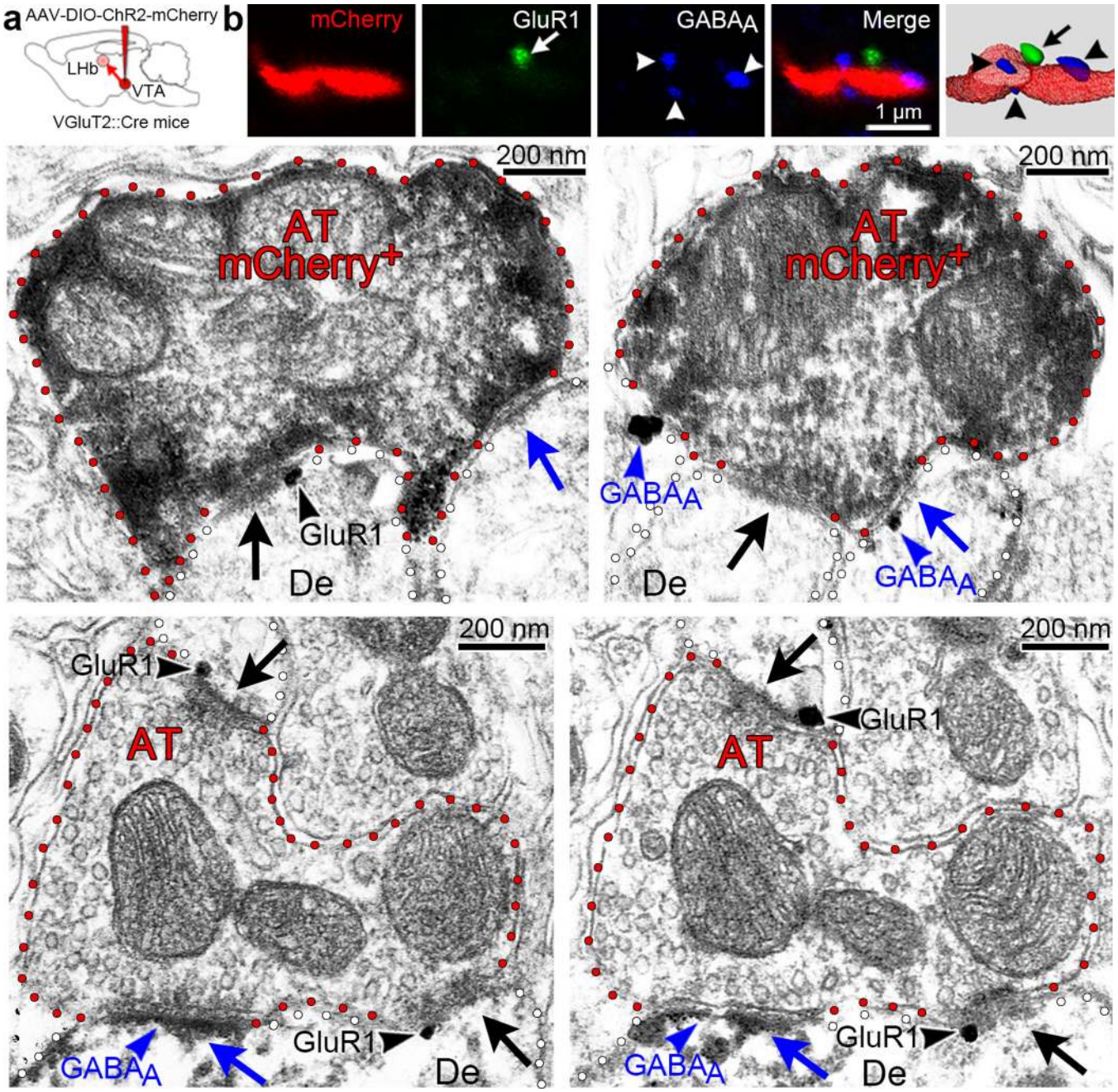


**Figure 3. Presence of both glutamatergic and GABAergic receptors postsynaptic to single mesohabenular axon terminals**

**a**, Cre-inducible AAV-DIO-ChR2-mCherry vector injected into VTA of VGluT2::Cre mice. Mesohabenular AT were identified by mCherry expression and examined under confocal (**b**) or electron microscopy (**c–f**). (**b**) Mesohabenular fiber expressing mCherry (red). Single focal planes are shown for immunolabeling of glutamate receptor 1 containing AMPA receptor (GluR1, green), $GABA_A$ receptor (blue), and merge. Far right panel is 3-D reconstruction of merged z-stacks showing GluR1 (arrow) and $GABA_A$ receptors (arrowheads) proximal to a mCherry-labeled mesohabenular fiber. (**c–d**) LHb sections from

VGluT2-ChR2-mCherry mouse showing mCherry detection by immunoperoxidase-labeling (scattered dark material) and detection of either GluR1 or $GABA_A$ receptor by immunogold. Experiments were repeated successfully three times. (**c**) Detection of GluR1(black arrowhead) at the asymmetric synapse (black arrow) postsynaptic to a mCherry-labeled AT that simultaneously forms a symmetric synapse (blue arrow). (**d**) Detection of $GABA_A$ receptor (blue arrowhead) at the symmetric synapse (blue arrow) postsynaptic to a mCherry-labeled AT that simultaneously forms an asymmetric synapse (black arrow). Experiments were repeated successfully three times. (**e–f**) Rat LHb serial sections. Detection of GluR1receptor by immunogold and detection of $GABA_A$ receptor by immunoperoxidase (scattered dark material). Detection of GluR1 (black arrowheads) at two asymmetric synapses (black arrows) postsynaptic to a mCherry-labeled AT that simultaneously forms a symmetric synapse containing $GABA_A$ receptor (blue arrowhead). Note the dendrite (De) establishing both symmetric and asymmetric synapses co-expressing GluR1 and $GABA_A$ receptors.

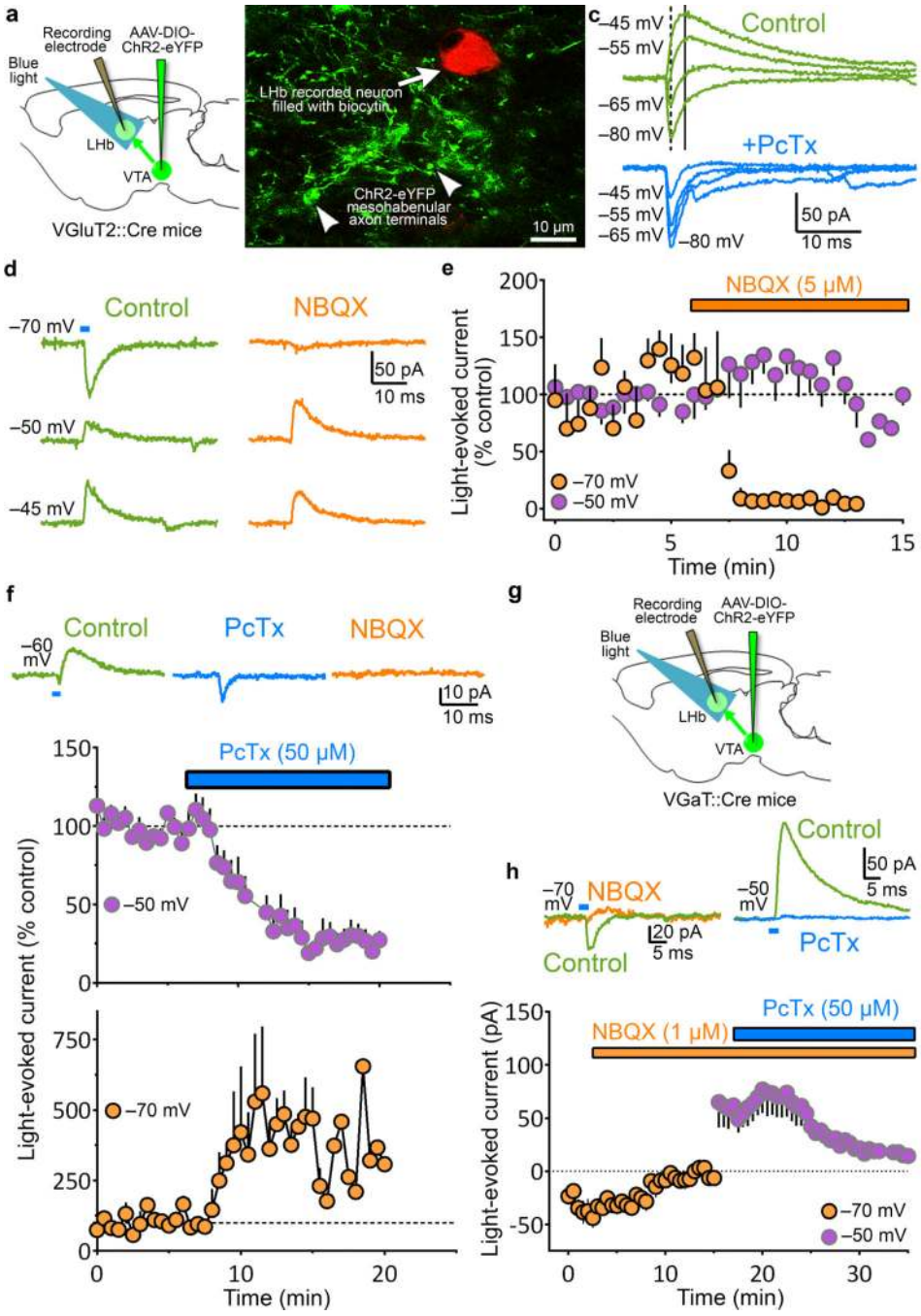


**Figure 4. Selective stimulation of mesohabenular terminals evokes both $GABA_A$ mediated outward and AMPA mediated inward currents in LHb neurons**

(**a**) Cre-inducible AAV-DIO-ChR2-eYFP vector injected into VTA of VGluT2::Cre mice. Light stimulation of ChR2-eYFP-fibers and LHb whole-cell recordings. (**b**) Recorded biocytin-filled LHb neuron intermingled with ChR2-eYFP-fibers. (**c**) Light pulses (473 nm; 5 ms) evoked inward and outward currents at varying holding potentials. Top: Light evoked both fast inward (dotted line) and slower outward currents (solid line). Light-evoked inward currents at hyperpolarized holding potentials (≈–70 mV), outward currents at depolarized

holding potentials (≈−50 mV), and both inward and outward currents at intermediate holding potentials (≈−60 mV). Outward, but not inward, currents were blocked by Picrotoxin (PcTx, 50 μM; $GABA_A$ receptor antagonist). (**d**) Inward currents were glutamatergic. Inward currents were abolished by AMPA receptor antagonist NBQX (5 μM) at −70 mV [**e**, summary; mean ± s.e.m. orange circles; paired t-test, t(3)=4.1; p = 0.026, n = 4 neurons from 4 VGluT2-ChR2 mice], but not at −50 mV (middle) or −45 mV (bottom). (**e**) Summary responses at −50 mV; purple circles, paired t-test, t(4)=0.64, p = 0.56, n = 5 neurons from 5 VGluT2-ChR2 mice. (**f**) GABAergic outward currents shunt glutamatergic inward currents. Top: both, light-evoked small inward and larger outward currents (left) in cells at −60 mV. PcTx eliminated the outward current and enhanced the inward (middle), which was eliminated by NBQX (right). Bottom: PcTx eliminated outward currents in all cells held at −50 mV [mean ± s.e.m.; purple circles; paired t-test, t(9)=6.2; p = 0.0002, n = 10 neurons from 8 VGluT2-ChR2 mice]. PcTx enhanced inward currents in cells held at −70 mV [mean ± s.e.m; orange circles; paired t-test, t(4)=2.9; p = 0.0437, n = 5 neurons from 5 VGluT2-ChR2 mice]. (**g**) Confirmation of glutamatergic-GABAergic co-transmission by mesohabenular AT, Cre-inducible AAV-DIO-ChR2-eYFP vector injected into VTA of VGaT::Cre mice. (**h**) Top left: Light-evoked inward current (control) at −70 mV was abolished by NBQX (1 μM) [summary in bottom; mean ± s.e.m. orange circles; paired t-test, t(5)=3.4; p = 0.0189, n = 6 neurons from 3 VGaT-ChR2 mice]. Top right: Outward current at −50 mV in the same cell before (control) and after PcTx [summary in bottom; mean ± s.e.m. purple circles; paired t-test, t(5)=3.0; p = 0.03, n = 6 neurons from 3 VGaT-ChR2 mice].

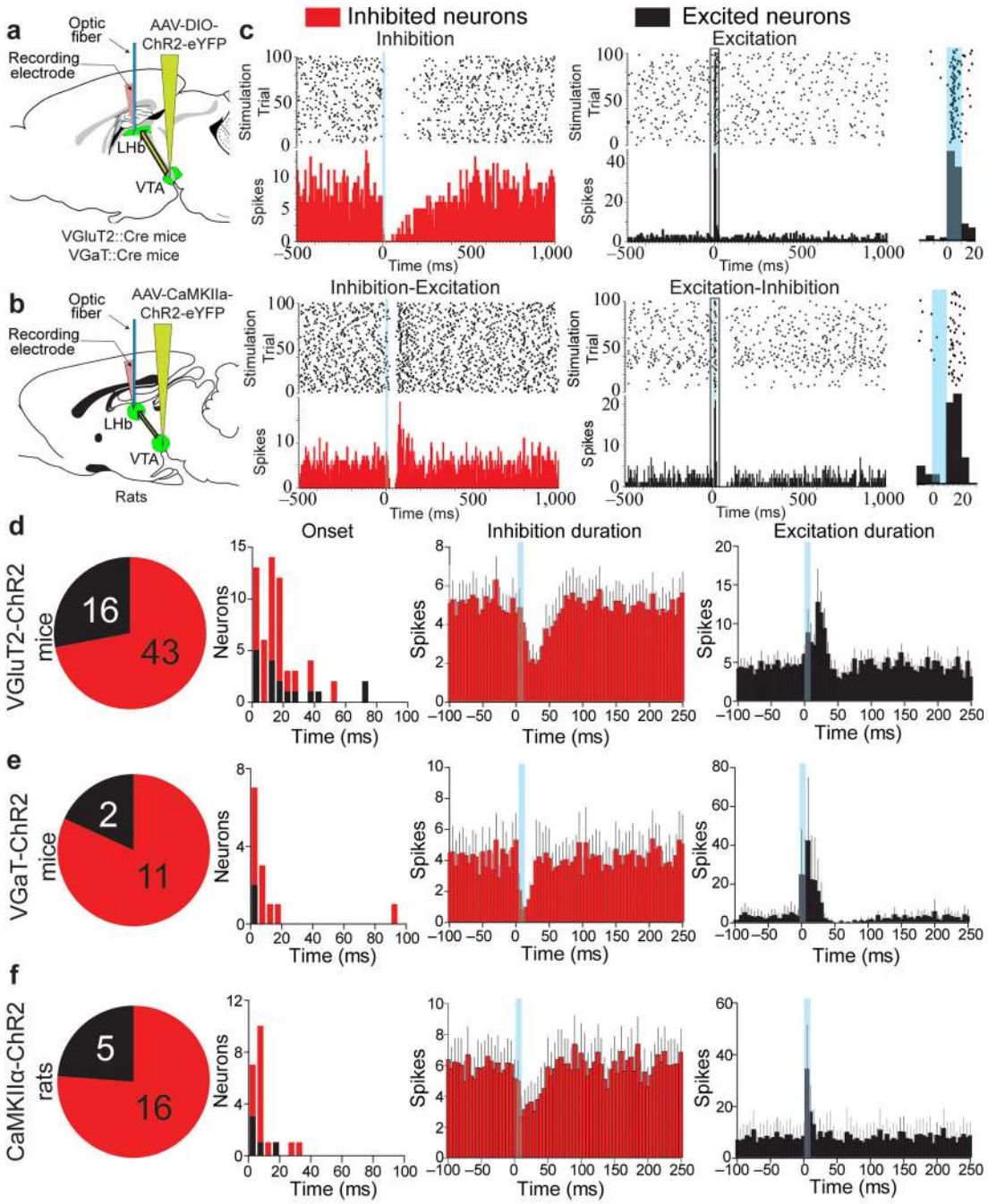


**Figure 5. In vivo optical stimulation of mesohabenular inputs evokes inhibition in most LHb neurons and evokes excitation in some**

(**a**) Cre-inducible AAV-DIO-ChR2-eYFP vector injected into VTA of VGluT2::Cre (VGluT2-ChR2 mice) or VGaT::Cre mice (VGaT-ChR2 mice). (**b**) AAV-CaMKIIα-ChR2-eYFP vector injected into VTA of rats (CaMKIIα-ChR2 rats). (**c–f**) LHb single-unit recordings and local optical stimulation (10 ms pulse; blue bars). (**c**) Four responses were found: a fast inhibition followed by slow return to pre-stimulation activity (inhibition), a fast inhibition followed by excitation (inhibition-excitation), a fast brief excitation (excitation) or

a fast brief excitation followed by inhibition (excitation-inhibition). Top panel shows rasters of timing of action potentials (black dots) for all optical stimulation sweeps and peristimulus time histograms (red or black bar graphs, bottom panels) aligned to optical stimulation onset. Insert (right) shows outlined portion of excited neurons' latency and jitter spike times in response to light stimulation. (**d–f**). Summary of light-evoked LHb responses (duration panels show mean ± s.e.m.) from VGluT2-ChR2 mice (n = 59 neurons from 16 mice; **d**), VGaT-ChR2 mice (13 neurons from 5 mice; **e**), and CaMKIIα-ChR2 rats (21 neurons from 9 rats; **f**).

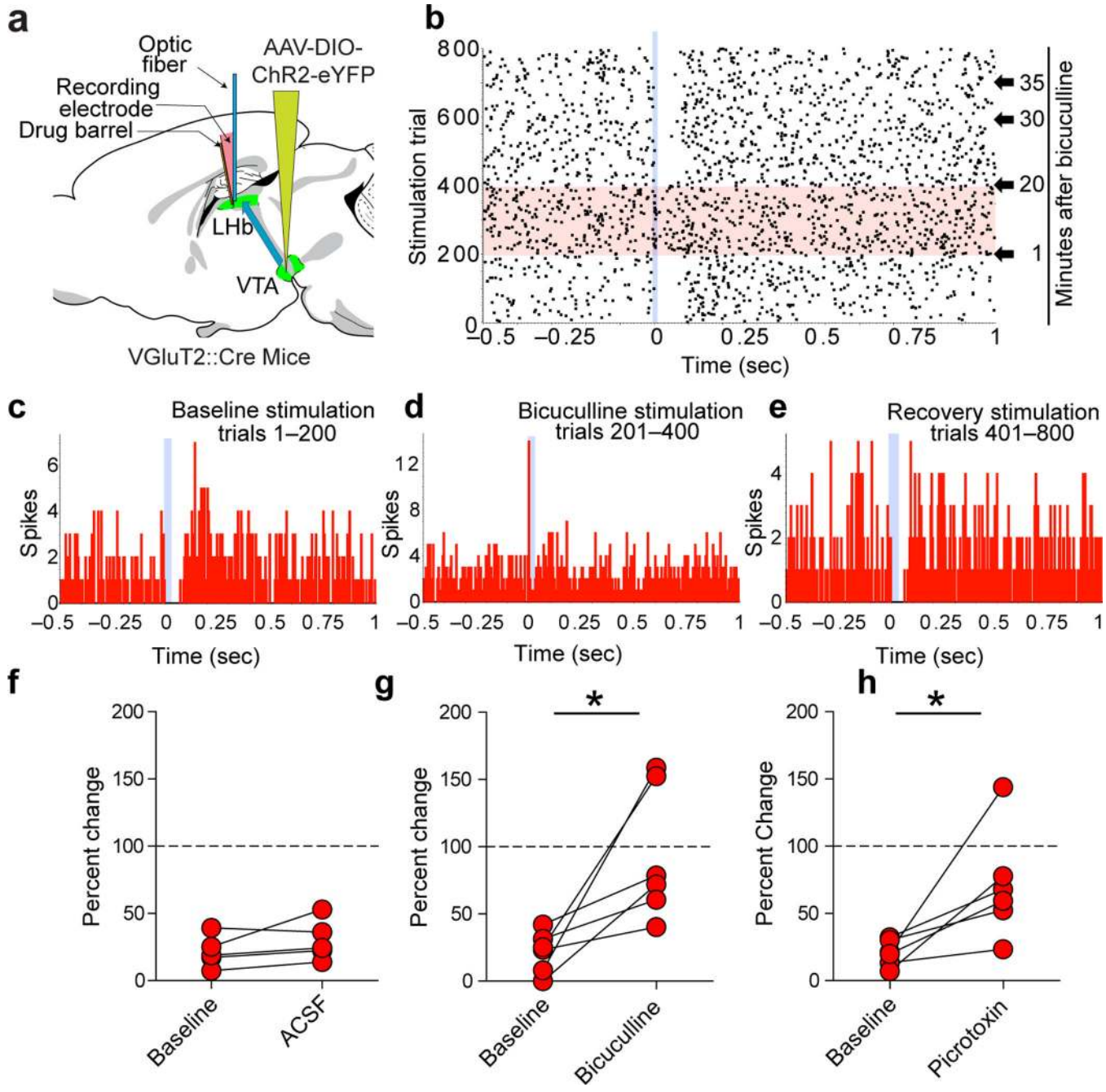


**Figure 6. Mesohabenular light-evoked inhibition is sensitive to $GABA_A$ antagonists *in vivo***

(**a**) Delivery of a Cre-inducible AAV-DIO-ChR2-eYFP vector into the VTA of VGluT2::Cre mice. An optical fiber and a drug barrel [filled with a $GABA_A$ antagonist, either picrotoxin (0.5 mM) or bicuculline (0.5 mM)] were glued to a glass electrode. Light pulses (473 nm; 10 ms) were delivered every 2 sec. (**b–e**) Inhibition of a LHb neuron in response to 10 ms mesohabenular fiber light stimulation (sweeps 1–200, raster in **b**, peristimulus time histogram (PSTH) in **c**). Local infusion of bicuculline (50 nl) blocked mesohabenular light-evoked inhibition (sweeps 201–400, raster in b, PSTH in **d**). The inhibition was recovered 20 min after application of bicuculline (sweeps 401–800, raster in b, PSTH in **e**). (**f–h**)

Population analysis of mesohabenular light-evoked inhibition. **f**, Percent change in firing rate evoked by mesohabenular fibers light stimulation before (baseline) and after artificial cerebral spinal fluid (ACSF). ACSF had no effect on light-evoked inhibition (paired t-test, $t(4) = 1.62$, $p = 0.18$, $n = 5$ neurons from 3 mice). (**g**) Percent change in firing rate evoked by mesohabenular fiber light stimulation before (baseline) and within 20 min of local infusion of bicuculline. Bicuculline significantly attenuated mesohabenular light-evoked inhibition (paired t-test, $t(5)=3.2$, $p = 0.024$, $n = 6$ neurons from 3 mice). (**h**) Percent change in firing rate evoked by mesohabenular fiber light stimulation before (baseline) and within 20 min of local infusion of picrotoxin. Picrotoxin significantly attenuated mesohabenular light-evoked inhibition (paired t-test, $t(6)=3.0$, $p = 0.03$, $n = 7$ neurons from 6 mice). *$p < 0.05$.

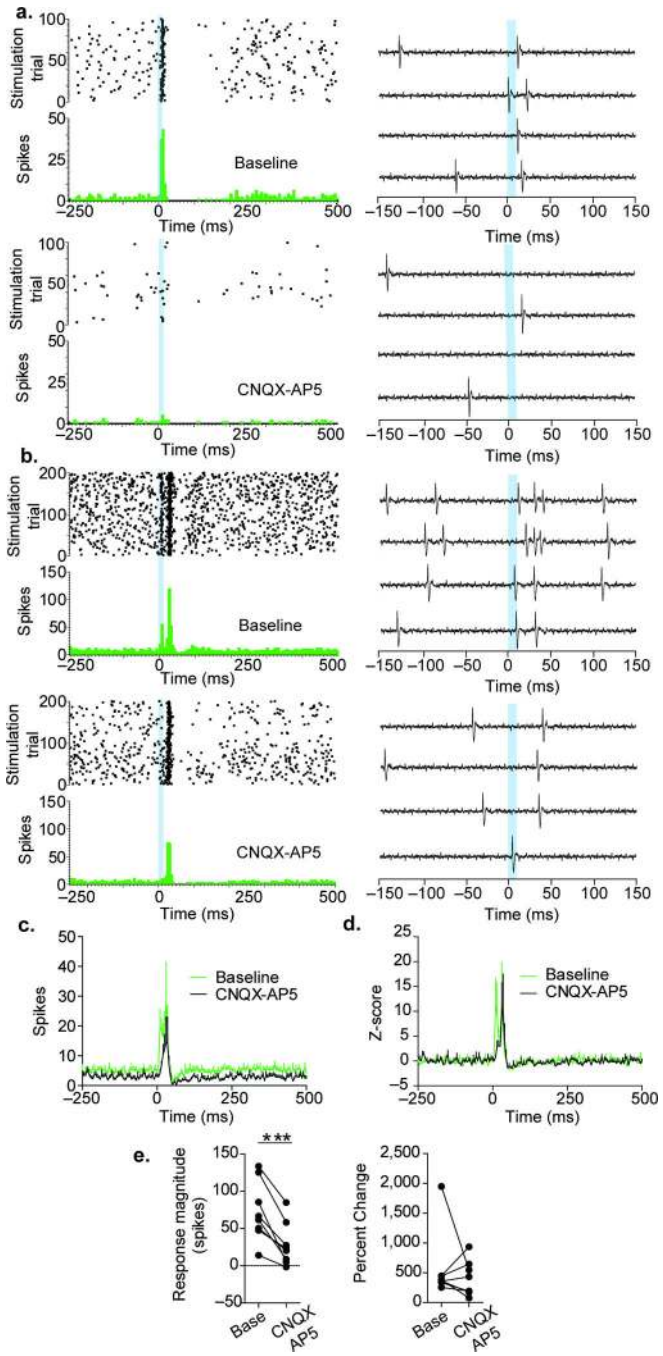


**Figure 7. Mesohabenular light-evoked excitation is sensitive to glutamate receptor antagonists *in vivo***

(**a–b**) Two examples of mesohabenular light-evoked excitation. Top and bottom panels show LHb neurons before and immediately after local infusion of a cocktail of the AMPA and NMDA receptor antagonists CNQX (50 μM) and AP5 (100 μM). Examples of raw signals recorded are shown on the right side panels. CNQX-AP5 blocked the mesohabenular-evoked excitation in neuron shown in **a**. The excitation occurring immediately after the laser stimulation in neuron shown in **b** was blocked by CNQX-AP5, a secondary delayed

excitation remained. (**c–e**) Population analysis of mesohabenular light-evoked excitation. (**c**) Changes in absolute spiking activity of LHb neurons. CNQX-AP5 decreased both spontaneous and mesohabenular light-evoked excitation. (**d**) After normalizing the firing activity of LHb neurons by their pre-stimulus spontaneous activity, two components of mesohabenular light-evoked excitation were evident: a fast component sensitive to CNQX-AP5 and a delayed component insensitive to CNQX-AP5. (**e**) Quantitative analysis of the mesohabenular light-evoked excitation. All LHb neurons showed a decrease in the number of spikes evoked by stimulation of mesohabenular fibers (paired t-test, $t(6) = 5.8$, $p = 0.0007$, left panel; n = 7 neurons from 4 VGluT2-ChR2 mice). In five neurons, CNQX-AP5 produced a larger decrease in mesohabenular light-evoked excitation relative to their spontaneous activity. In three neurons, CNQX-AP5 produced a decrease in the spontaneous activity that was larger than those observed on the mesohabenular light-evoked excitation, resulting in an increase in the percent change (right panel). ***$p < 0.001$.

**Table 1**

Mesohabenular neurons expressing VGluT2 mRNA, GAD mRNA or TH-immunoreactivity

| | VGluT2$^+$ GAD$^+$ TH$^-$ | VGluT2$^+$ GAD$^+$ TH$^+$ | VGluT2$^+$ GAD$^-$ TH$^+$ | VGluT2$^+$ GAD$^-$ TH$^-$ | VGluT2$^-$ GAD$^+$ TH$^-$ | VGluT2$^-$ GAD$^-$ TH$^+$ | VGluT2$^-$ GAD$^+$ TH$^+$ | VGluT2$^-$ GAD$^-$ TH$^-$ |
|---|---|---|---|---|---|---|---|---|
| Rat # 2 | 55.3% (*n* = 105) | 25.8% (*n* = 49) | 4.7% (*n* = 9) | 7.4% (*n* = 14) | 2.6% (*n* = 5) | 1.6% (*n* = 3) | 0.5% (*n* = 1) | 2.1% (*n* = 4) |
| Rat # 3 | 59.8% (*n* = 98) | 22.6% (*n* = 37) | 8.5% (*n* = 14) | 4.9% (*n* = 8) | 2.4% (*n* = 4) | 0.6% (*n* = 1) | 0.0% (*n* = 0) | 1.2% (*n* = 2) |
| Rat # 5 | 55.3% (*n* = 68) | 20.3% (*n* = 25) | 7.3% (*n* = 9) | 6.5% (*n* = 8) | 5.7% (*n* = 7) | 2.4% (*n* = 3) | 0.8% (*n* = 1) | 1.6% (*n* = 2) |
| Mean ± S.E.M. | 56.8 ± 1.5% (*n* = 271) | 22.9 ± 1.6% (*n* = 111) | 6.9 ± 1.1% (*n* = 32) | 6.3 ± 0.7% (*n* = 30) | 3.6 ± 1.1% (*n* = 16) | 1.5 ± 0.5% (*n* = 7) | 0.4 ± 0.2% (*n* = 2) | 1.7 ± 0.3% (*n* = 8) |

Percent refers to the number of FluoroGold retrogradely labeled VTA neurons co-expressing VGluT2 mRNA, GADs mRNA, or TH-immunofluorescence divided by the total number of FluoroGold labeled VTA neurons. Numbers in parentheses refer to number of counted neurons in that phenotype condition. FG-VTA cell counting was made in 9 or 10 sections, each from rats #2, #3, and #5 (n = 3 rats; Supplementary Figure 1), between bregma −4.9 mm and −6.1 mm.